PRELIMINARY RESULTS FROM THREE YEARS OF UAS-BASED GNSS-R FIELD CAMPAIGN OVER AGRICULTURAL FIELDS FOR FIELD-SCALE SOIL MOISTURE RETRIEVAL

Md Mehedi Farhad[1], *Volkan Senyurek*[1], *Mohammad Abdus Shahid Rafi*[1], *Ardeshir Adeli*[2], *Mehmet Kurum*[3], *and Ali Cafer Gurbuz*[1]

[1] Mississippi State University, Mississippi State, MS, USA
[2] USDA Genetics and Sustainable Agriculture Research Unit Starkville MS, USA
[3]University of Georgia, Athens, GA, USA

ABSTRACT

Unmanned Aircraft Systems (UAS) play an essential role in providing high-resolution information for precision agriculture (PA). Global Navigation Satellite System (GNSS) Reflectometry (GNSS-R) from a UAS can provide higher spatial and temporal resolution for soil moisture (SM) retrievals. This study summarizes and analyzes of a three-year-long field campaign including comprehensive GNSS-R and ancillary data from crop fields. The field data collections were conducted on 210 by 110 m (2.31 ha) corn and cotton fields over 3 years from 2021 to 2023. The results indicate that high-resolution SM measurement can be achieved with a low-cost GNSS-R system onboard a mid-size UAS platform for use in PA applications.

Index Terms— GNSS-R, Soil moisture, UAS

1. INTRODUCTION

Unmanned Aircraft Systems (UAS) play an essential role in providing high-resolution information for precision agriculture (PA) [1]. Accurate and high-resolution soil moisture (SM) measurement is one of the critical inputs for site-specific PA management. Efficient irrigation management enhances crop quality, yield, and resource conservation [2]. Using SM probes is a traditional and reliable method for accurately measuring volumetric soil moisture [3]. However, high-resolution SM observations through SM probes can be time-consuming, costly, and inefficient for large heterogeneous fields.

UAS-based technologies have various applications in PA, such as vegetation trait and stress monitoring [4], weed mapping [5], and irrigation management [6]. However, SM measurements using UAS are currently very limited and not yet fully developed. Several existing UAS-based SM estimation studies aim to obtain field-level SM results. These studies are mainly based on optical sensing focused on soil or vegetation spectral reflectance from UAS. Soil spectral reflectance studies showed that reflectance level decreases as SM increases due to a darkening of the soil surface color [7]. The main drawbacks of soil spectral reflectance are that the performance depends only on soil color and texture, while SM is affected by many factors. In addition, the penetration depth of the optical sensing is highly limited to the uppermost layer of soil, and the sensing modality requires atmospheric compensation for higher sensitivity. Using an inversion model of SM based on vegetation spectral indices is an alternative for SM retrieval. The principle is to use remotely sensed spectral observations strongly linked with SM [8]. The studies show that many canopy spectral indices and biophysical and biochemical parameters are strongly correlated with SM [9]. However, this technique observes vegetation rather than the soil, depends on vegetation type and fertilizer usage, and is not available for barren and sparsely vegetated areas. Additionally, changes in spectral indices can lag changes in climate/irrigation/precipitation. This lag may vary between 20 and 45 days depending on vegetation type [10]. As an alternative, radio frequency (RF) signals transmitted by Global Navigation Satellite System (GNSS) satellites at L-band frequencies can penetrate soil and the reflections are sensitive to SM in the top 5 cm depth [11]. The ability of GNSS-R to sense SM has already been demonstrated from space-borne [12], airborne [13], UAS-based [14], and tower platforms [15]. Many research groups have developed models and algorithms to retrieve SM from land observations using NASA's recent spaceborne GNSS-R mission, Cyclone Global Navigation Satellite System (CYGNSS) [16, 17]. Although global CYGNSS-based SM estimations have shown high correlation with SM observations of Soil Moisture Active Passive (SMAP), it has spatial resolutions of several kilometers, and because of this reason it is not directly usable for PA which requires sub-field level SM information.

To bring the GNSS-R technique into PA applications, we utilize a low-altitude (15 m) mid-size UAS equipped with a GNSS receiver, which collects signals only reflected from the

This work was supported by U.S. National Science Foundation (NSF) under Grant # 2142218

land surface. In this article, we summarized three years of UAS-based GNSS-R data collection campaign and analyzed calculated surface reflectivity compared to in-situ SM measurements. Our initial findings indicate that the surface reflectivity calculated using GNSS-R was closely correlated with the measured SM, with a correlation coefficient ranging from 0.65 to 0.71.

2. METHODOLOGY

Our research objective is to explore the feasibility of employing an off-the-shelf, cost-effective GNSS receiver and a UAS platform for the retrieval of high-resolution surface SM at the field scale using the GNSS-R technique. We demonstrated the practicability of this technique in [18]. The measurement methodology entails attaching a GNSS receiver to a small UAS platform, with a downward-facing GNSS receiver antenna positioned beneath the UAS on an 18-inch meshed plate. This arrangement ensures that the GNSS receiver acquires only the ground-reflected GNSS signal, with the direct signal obstructed by the meshed ground plate. Another identical GNSS receiver is positioned in an unobstructed open-sky area to capture the direct GNSS signal for future analysis. The L1-band (1575.42 MHz) GNSS signal having a wavelength of $\sim$ 19.5-cm penetrates the soil up to $\sim$ 5-cm. The airborne GNSS receiver receives these ground-reflected signals using its onboard receiver system. The simplified measurement configuration is shown in Fig. 1.

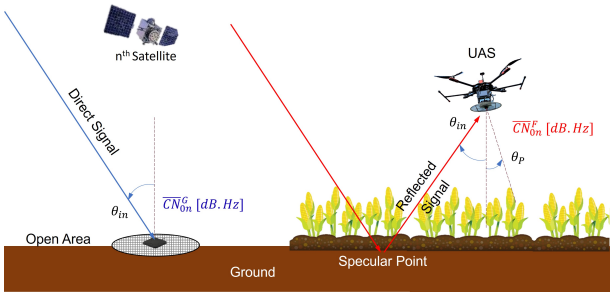

Fig. 1: Simplified structure of the proposed approach. UAS collects reflected GNSS signals from the specular points via U-blox GNSS receiver.

2.1. Instruments

In this experiment, we employed a custom mid-size UAS platform constructed from carbon fiber. The UAS can carry approximately 20 pounds as payload during a 15-minute flight. The GNSS receiver used in the experiment is the U-blox application board, accompanied by its L-band linear polarized antenna. This antenna is affixed to an 18-inch meshed ground plate made of aluminum (resembling a pizza pan). The GNSS receiver antenna is positioned in a downward-facing orientation to maximize the reception of ground-reflected GNSS signals. For the reference, an identical U-blox GNSS receiver and a linear antenna were used. However, the antenna for the reference receiver is upward-facing and placed on top of an 18-inch meshed ground plate, enabling it to receive only the direct, unobstructed GNSS signal.

2.2. Study field and data collection

2.2.1. *Study Area Description*

The investigation was conducted in a field measuring 210 m by 110 m (2.31 ha), located at the R. R. Foil Plant Science Research Center, Mississippi State University, Starkville, MS, USA, with coordinates at the lower left corner $33^o28^{'}15.70^{"}N$ and $88^o46^{'}27.53^{"}W$. Figure 2 exhibits the flight paths over the defined field area and a nearby water body for the data collection in this study. The average annual precipitation is around 1,329 mm, and humidity fluctuates between 55% and 66% monthly. The field is situated at an elevation of 92 m above sea level, featuring rows spaced 96.5 cm apart. The North side of the study field comprises a large water body and a small creek. Table 1 shows the crop planting changes through the 3-year experiment period.

2.2.2. *Data Collection*

A total of 337 GNSS-R flights were performed during the study period at an altitude of 15m with a flight speed of 5m/s. Besides GNSS-R data, we collect multispectral images and LIDAR point cloud data weekly, using MicaSense RedEdge MX and Geocue TrueView 51, respectively. The data collection flight statistics over the years are highlighted in Table 2.

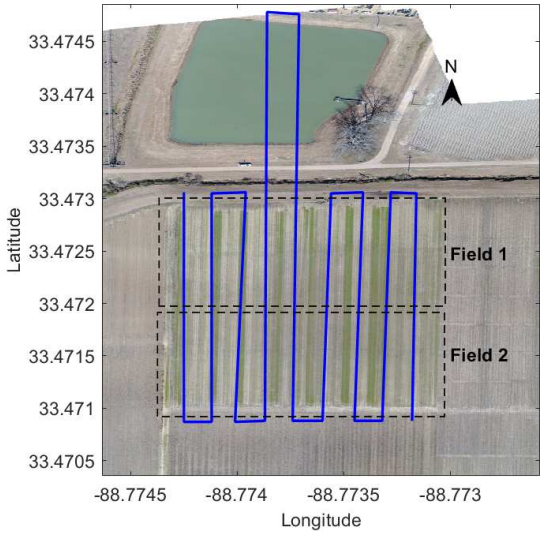

Fig. 2: Flight path of the data collection: a total of 9 flight lines in the North-South direction cover both field 1 and field 2. Middle 2 lines pass over a water body.

2.2.3. *In-situ Data Collection*

The ground truth SM data was collected by EC-5 volumetric water content sensors using the capacitance method and manufactured by METER Group Inc., Pullman, WA, USA. Sensors were placed in different locations in the study field. Each

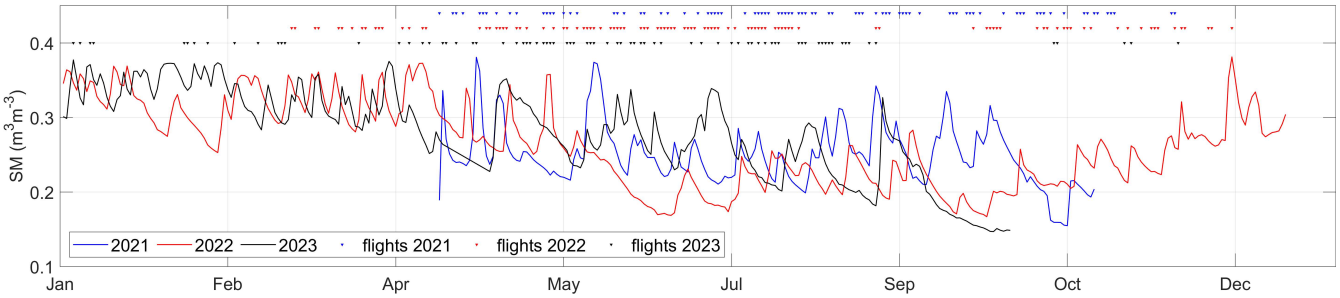

Fig. 3: Average measured in-situ SM of the study field for different years (2021-2023) and available flights of each year.

Table 1: Field-Section, Plantation, and Harvest Timeline of the Crops.

Year	Crop Type	Field Section	Plantation Time	Harvest Time
2021	Corn	South / Field 2	April 07	September 17
	Cotton	North / Field 1	May 23	November 05
2022	Corn	North / Field 1	March 28	September 08
	Cotton	South / Field 2	April 29	October 18
2023	Corn	South / Field 2	April 20	September 12
	Cotton	North / Field 1	May 16	October 18

Table 2: Flights and statistics of collected data

	Year	2021	2022	2023 (up to Aug.)
# of flights	GNSS-R	122	136	79
	Multispectral	40	45	40
	LIDAR	34	27	21
GNSS-R data	# of PNR	3,369	3,029	1,361
	# of Specular Point	1,761,126	1,853,839	670,151
	# of SM probe	16	26	19

probe provides SM measurements for the top 5 cm SM every three hours. All SM probes were kept in the field throughout the year except for cover and main crop planting and harvesting periods. Fig. 3 shows the average measured SM of the study field through the experiment years.

2.3. GNSS-R data extraction

A GNSS receiver on the UAS receives and processes signals sent by GNSS satellites. As an output, a GNSS receiver provides National Marine Electronics Association (NMEA) messages, which is a standard data and communication format for electronic instruments, including GNSS receivers. GNSS receivers' NMEA messages provide time, position, velocity, and satellite information. From recorded NMEA messages, we have decoded RMC (recommended minimum specific GPS/Transit data) and GSV (satellites in view) messages to extract the date/time information of the receiver and in-view satellite information, respectively. From the GSV message, we obtained the pseudo-random noise (PRN) number, which is an identification number, elevation, azimuth, and signal strength value, carrier-to-noise density ratio (C/N_0), for each visible GNNS satellite.

2.4. UAS telemetry data and specular point calculation

Besides GNSS-R measurements, we also save the UAS telemetry data during each flight campaign. The flight controller of UAS saves all telemetry data to the controller's onboard memory at a 20Hz sampling rate. From telemetry data, we extracted data/time, UAS orientation pitch, roll and yaw, and location information latitude, longitude, and altitude. Then, we aggregated both datasets (GNSS-R and telemetry) based on time stamps.

In the assumption of coherent surface reflection, we determined all specular reflection points (SP) by using local plane reflection approximation theory for each reflected signal using the position of the UAS and the GNSS satellites. We have used the elevation and azimuth angles information obtained from the GNSS receiver to calculate SPs.

3. RESULTS

GNSS-R is a type of passive bistatic radar configuration that involves the acquisition of reflected signals from the Earth's surface by a GNSS receiver. The main measurement taken for remote sensing is the power of the reflected signal that reaches the receiver. In most land observations, there is a significant coherent component in the signal, which means that the received signal power can be calculated in a formalized manner, as described in [19].

$$P_r = \frac{P_t G_t}{4\pi (R_{ts} + R_{sr})^2} \frac{G_r \lambda^2}{4\pi} \Gamma \tag{1}$$

, where P_t represents the transmitted power, G_t, is the gain of the transmitting antenna, R_{ts} is the distance between the transmitter and the specular reflection point, R_{sr} is the distance between the specular reflection point and the receiver. In UAS-based GNSS-R, the distance from specular points to receiver R_{ts} is much smaller compared to the distance of specular points to the transmitter. Γ is the surface reflectivity, G_r is the gain of the receiving antenna, and λ is the GPS wavelength (0.19 m).

3.1. Surface reflectivity calculation from C/N_0

Reflected signal power, which is measured from a UAS platform, is not only a function of SM but also multiple factors that can affect received signal power, such as the transmitted power of GNSS satellites, the distance between the satellite and the SP, and the receiver antenna pattern/gain. On the field side, surface roughness and vegetation effects are two main factors. In our flight path, we included a 0.9 ha area of the irrigation reservoir that has a known reflection coefficient. Using reflected measurements from this surface will help eliminate unknown incident power variations such as transmitter power, distance, elevation angle, and receiver antenna gain.

The reflection coefficient in the perpendicular polarization case for nonmagnetic dielectric media can be calculated as,

$$\Gamma_{\perp} = \frac{cos\theta_i - \sqrt{\epsilon_2/\epsilon_1 - sin^2\theta_i}}{cos\theta_i + \sqrt{\epsilon_2/\epsilon_1 - sin^2\theta_i}} \quad (2)$$

where, ϵ_2 and ϵ_1 are the relative permittivity of water (81) and air(1), respectively. θ_i is the incident angle. We have calculated the water reflectivity for the viable GNSS satellites using incident angle during flight. We can formalize the measured C/N_0 over the water and land as,

$$C/N_{0_{\text{pnr}}}^{\text{water}}[\text{dB.Hz}] = G_r(\theta,\phi)[\text{dB.Hz}] + \Gamma(\theta)_{\text{pnr}}^{\text{water}}[\text{dB}] \quad (3)$$

$$C/N_{0_{\text{pnr}}}^{\text{land}}[\text{dB.Hz}] = G_r(\theta,\phi)[\text{dB.Hz}] + \Gamma(\theta)_{\text{pnr}}^{\text{land}}[\text{dB}] \quad (4)$$

where, $G_r(\theta,\phi)$ is the angle-dependent antenna factor, $\Gamma(\theta)_{\text{pnr}}^{\text{water}}$ is the calculated water reflectivity and $\Gamma(\theta)_{\text{pnr}}^{\text{land}}$ is the estimated land reflectivity. If we ignore small UAS orientation differences over the flight, the antenna factor will be the same for the water and land. We can estimate land surface reflectivity as,

$$\Gamma(\theta)_{\text{pnr}}^{\text{land}}[\text{dB.Hz}] = C/N_{0_{\text{pnr}}}^{\text{land}}[\text{dB.Hz}] - [\overline{C/N_0}_{\text{pnr}}^{\text{water}}[\text{dB.Hz}] - \Gamma(\theta)_{\text{pnr}}^{\text{water}}[\text{dB}]] \quad (5)$$

,where, $\overline{C/N_0}_{\text{pnr}}^{\text{water}}$ is the average measured C/N_0 over the water for each PNR. The equation 5 not only calibrates the receiver antenna factor but also adjusts for incident power variations caused by differences in transmitter power and distance.

3.2. Correlation with in-situ SM

Table 3 displays the correlation coefficient between estimated surface reflectivity and the averaged SM of crop fields. The daily average SM of crop fields is determined by taking in-situ measurements from all available probes in the area during flights. In the same manner, we averaged the estimated reflectivity of the specular points daily for each crop field. The results show that the estimated reflectivity is positively correlated with ground truth SM measurements for both crop fields and different years except for the cotton field in 2021. There were only 8 SM probes in the cotton field in 2021, and the limited number of in-situ SM probes in the area may not accurately represent the overall SM of the cotton field in 2021.

Table 3: Correlation coefficient of estimated reflectivity with measured average SM.

	Corn		Cotton	
	R	#of days	R	#of days
2021	0.70	60	0.39	66
2022	0.71	91	0.71	93
2023	0.65	45	0.71	39

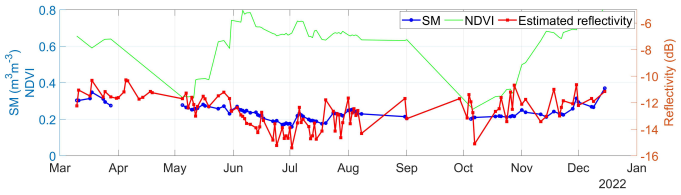

(a) Corn

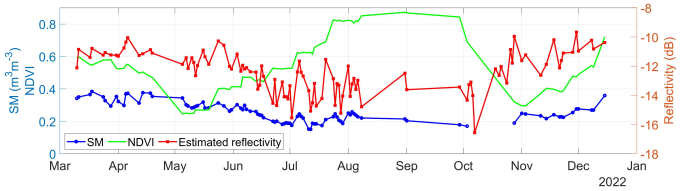

(b) Cotton

Fig. 4: Estimated average surface reflectivity, NDVI, and averaged measured SM for 2022 flight days. (a) corn, (b) cotton field.

Figure 4 provides a temporal comparison of UAS-based reflectivity estimation against SM probe measurements for 2022. We averaged daily specular point reflectivity estimations and SM probe measurements of each crop field. This figure shows that estimated reflectivity closely follows the in-situ measurements for both crop fields.

4. CONCLUSION

In this study, we demonstrated that the use of GNSS-R data collected via UASs can be leveraged to determine surface reflectivity, which is a proxy measure of surface SM. We applied a correction procedure to eliminate unknowns such as transmitter power, distance, and antenna factor by using water body measurements. In this study, we did not include other factors, such as vegetation biomass, surface roughness, and receiver antenna orientation changes. Ongoing efforts correct these factors with ancillary data to estimate soil moisture at a subfield scale.

5. REFERENCES

[1] Susha Lekshmi SU, DN Singh, and Maryam Shojaei Baghini, "A critical review of soil moisture measurement," *Measurement*, vol. 54, pp. 92–105, 2014.

[2] JW Knox, MG Kay, and EK Weatherhead, "Water regulation, crop production, and agricultural water management—understanding farmer perspectives on irrigation efficiency," *Agricultural water management*, vol. 108, pp. 3–8, 2012.

[3] Viacheslav I Adamchuk, J W Hummel, MT Morgan, and SK Upadhyaya, "On-the-go soil sensors for precision agriculture," *Computers and electronics in agriculture*, vol. 44, no. 1, pp. 71–91, 2004.

[4] Martin Peter Christiansen, Morten Stigaard Laursen, Rasmus Nyholm Jørgensen, Søren Skovsen, and René Gislum, "Designing and testing a uav mapping system for agricultural field surveying," *Sensors*, vol. 17, no. 12, pp. 2703, 2017.

[5] Huasheng Huang, Yubin Lan, Aqing Yang, Yali Zhang, Sheng Wen, and Jizhong Deng, "Deep learning versus object-based image analysis (obia) in weed mapping of uav imagery," *International Journal of Remote Sensing*, vol. 41, no. 9, pp. 3446–3479, 2020.

[6] Catalina Albornoz and Luis Felipe Giraldo, "Trajectory design for efficient crop irrigation with a uav," in *2017 IEEE 3rd Colombian Conference on Automatic Control (CCAC)*. IEEE, 2017, pp. 1–6.

[7] Sophie Fabre, Xavier Briottet, and Audrey Lesaignoux, "Estimation of soil moisture content from the spectral reflectance of bare soils in the 0.4–2.5 μm domain," *Sensors*, vol. 15, no. 2, pp. 3262–3281, 2015.

[8] Leila Hassan-Esfahani, Alfonso Torres-Rua, Austin Jensen, and Mac McKee, "Assessment of surface soil moisture using high-resolution multi-spectral imagery and artificial neural networks," *Remote Sensing*, vol. 7, no. 3, pp. 2627–2646, 2015.

[9] Jingzhe Wang, Jianli Ding, Aerzuna Abulimiti, and Lianghong Cai, "Quantitative estimation of soil salinity by means of different modeling methods and visible-near infrared (vis–nir) spectroscopy, ebinur lake wetland, northwest china," *PeerJ*, vol. 6, pp. e4703, 2018.

[10] René R Colditz, Violeta L Arriola Villanueva, Inder Tecuapetla-Gómez, and Leticia Gómez Mendoza, "Temporal relationships between daily precipitation and ndvi time series in mexico," in *2017 9th International Workshop on the Analysis of Multitemporal Remote Sensing Images (MultiTemp)*. IEEE, 2017, pp. 1–4.

[11] KG Kostov and BI Vichev, "Passive microwave remote sensing of soils and vegetation—experimental and modeling results," in *Microwave Physics and Techniques*, pp. 251–266. Springer, 1997.

[12] Clara Chew, Rashmi Shah, Cinzia Zuffada, George Hajj, Dallas Masters, and Anthony J Mannucci, "Demonstrating soil moisture remote sensing with observations from the uk techdemosat-1 satellite mission," *Geophysical Research Letters*, vol. 43, no. 7, pp. 3317–3324, 2016.

[13] Alejandro Egido, Simonetta Paloscia, Erwan Motte, Leila Guerriero, Nazzareno Pierdicca, Marco Caparrini, Emanuele Santi, Giacomo Fontanelli, and Nicola Floury, "Airborne gnss-r polarimetric measurements for soil moisture and above-ground biomass estimation," *IEEE Journal of Selected Topics in Applied Earth Observations and Remote Sensing*, vol. 7, no. 5, pp. 1522–1532, 2014.

[14] Mehmet Kurum, Md. Mehedi Farhad, and Ali Cafer Gurbuz, "Integration of smartphones into small unmanned aircraft systems to sense water in soil by using reflected gps signals," *IEEE Journal of Selected Topics in Applied Earth Observations and Remote Sensing*, vol. 14, pp. 1048–1059, 2021.

[15] Kristine M Larson, John J Braun, Eric E Small, Valery U Zavorotny, Ethan D Gutmann, and Andria L Bilich, "Gps multipath and its relation to near-surface soil moisture content," *IEEE Journal of Selected Topics in Applied Earth Observations and Remote Sensing*, vol. 3, no. 1, pp. 91–99, 2009.

[16] V. Senyurek, F. Lei, D. Boyd, M. Kurum, A. Gurbuz, and R. Moorhead, "Machine learning-based cygnss soil moisture estimates over ismn sites in conus," *Remote Sensing*, vol. 12, no. 7, pp. 1168, 2020.

[17] M M Nabi, Volkan Senyurek, Fangni Lei, Mehmet Kurum, and Ali Cafer Gurbuz, "Quasi-global assessment of deep learning-based cygnss soil moisture retrieval," *IEEE Journal of Selected Topics in Applied Earth Observations and Remote Sensing*, vol. 16, pp. 5629–5644, 2023.

[18] Md Mehedi Farhad, Mehmet Kurum, and Ali Cafer Gurbuz, "A ubiquitous gnss-r methodology to estimate surface reflectivity using spinning smartphone onboard a small uas," *IEEE Journal of Selected Topics in Applied Earth Observations and Remote Sensing*, vol. 16, pp. 6568–6578, 2023.

[19] C. Chew and E. Small, "Description of the UCAR/CU soil moisture product," *Remote Sensing*, vol. 12, no. 10, pp. 1558, 2020.